


## Entanglement-variational hardware-efficient ansatz for eigensolvers

Xin Wang,<sup>1,2</sup> Bo Qi<sup>1,2,\*</sup>, Yabo Wang<sup>1,2</sup> and Daoyi Dong<sup>3</sup>

<sup>1</sup>Key Laboratory of Systems and Control, Academy of Mathematics and Systems Science, Chinese Academy of Sciences, Beijing 100190, People's Republic of China

<sup>2</sup>University of Chinese Academy of Sciences, Beijing 100049, People's Republic of China

<sup>3</sup>CIICADA Lab, School of Engineering, Australian National University, Canberra, ACT 2601, Australia

 (Received 8 November 2023; revised 11 March 2024; accepted 14 March 2024; published 27 March 2024)

Variational quantum eigensolvers (VQEs) are one of the most important and effective applications of quantum computing, especially in the current noisy intermediate-scale quantum (NISQ) era. There are two main approaches for VQEs: problem-agnostic and problem-specific. For problem-agnostic methods, they often suffer from trainability issues. For problem-specific methods, their performance usually relies upon the choice of initial reference states, which are often hard to determine. In this paper, we propose an entanglement-variational hardware-efficient ansatz (EHA), and numerically compare it with some widely used ansatzes by solving benchmark problems in quantum many-body systems and quantum chemistry. Our EHA is problem-agnostic and hardware-efficient, is especially suitable for NISQ devices, and has potential for wide applications. Our EHA can achieve a higher level of accuracy in finding ground states and their energies in most cases, even compared with problem-specific methods. The performance of the EHA is robust to the choice of initial states and to parameter initialization, and it has the ability to quickly adjust the entanglement to the required amount, which is also the fundamental reason for its superiority.

DOI: [10.1103/PhysRevApplied.21.034059](https://doi.org/10.1103/PhysRevApplied.21.034059)

### I. INTRODUCTION

Quantum computing has the potential to revolutionize many fields, including quantum many-body physics [1–3], quantum chemistry [4–6], materials science [7–9], and so on [10,11]. Among these, finding ground states and the corresponding energies of their Hamiltonians is a fundamental problem [1–5]. In the current noisy intermediate-scale quantum (NISQ) era [12–14], variational quantum eigensolvers (VQEs) [15–19] have been proposed to solve this problem, with the hope that approximate solutions could be found for large systems which are intractable with classical computers.

VQEs work in a hybrid quantum-classical manner [20]. They employ a parameterized quantum circuit (PQC) to generate parameterized trial states, and the variational parameters are updated by a classical optimizer through minimizing the objective function, which in general is the expectation value of the Hamiltonian with respect to the trial state.

To enhance the performance of VQEs, various methods have been developed from different perspectives. These include designing appropriate ansatzes for quantum circuits [21–27], tailored initial states [28,29], proper

parameter initializations [30,31], developing efficient optimization methods [32], employing feedback for iterations [33], and utilizing classical postprocessing with neural networks [34], among others [35–37]. It is clear that the ansatz of a quantum circuit directly determines the success of VQEs. For instance, if the quantum circuit is poorly expressible and thus cannot generate trial states close to the target state, then no other auxiliary methods can improve its performance [38,39]. There are mainly two ways to design ansatzes for quantum circuits: problem-agnostic and problem-specific [16].

The hardware-efficient ansatz (HEA) is a well-known and widely used problem-agnostic method, which seeks to minimize the hardware noise by using native gates and connectives [40–42]. When training quantum circuits based on HEAs, one often faces many challenges. Shallow HEA circuits are poorly expressible, and may cause the landscape of the cost function to be swamped with spurious local minima under global measurements [43,44]. Deep circuits, however, will make the PQC too expressive, resulting in barren plateaus (BPs) [45,46], i.e., the cost gradient is exponentially small with the number of qubits and/or the circuit depth. Both of these issues will make PQC training extremely difficult. A major reason is that in most existing HEAs, the entanglers are usually fixed, resulting in a lack of freedom to quickly adjust the entanglement of the trial states to the required amount. It is clear

\*Corresponding author. [qibo@amss.ac.cn](mailto:qibo@amss.ac.cn)

that the nature of the circuit ansatz determines the level of entanglement that can be achieved. On the one hand, generating a matched amount of entanglement is necessary to guarantee the convergence of eigensolvers based on HEAs. On the other hand, while entanglement can usually be quickly generated within a few layers, the excess entanglement cannot be removed efficiently [47]. It has been pointed out [48] that if the generated entanglement does not match the problem under study, it may hamper the convergence process. Moreover, it was argued [49] that too much entanglement can result in BPs. In addition, it was stated [50] that, even for shallow circuits, entanglement satisfying the volume law should be avoided.

To address the training issues of PQCs, it has been suggested to design circuit ansatzes in a problem-specific manner. Examples include the Hamiltonian variational ansatz (HVA), also commonly referred to as a Trotterized adiabatic state preparation ansatz [51], and the hardware symmetry-preserving ansatz proposed in Ref. [52], which reduces the explored space of unitaries through symmetry preservation and is referred to as the hardware symmetry-preserving ansatz (HSA) in our paper.

In quantum computational chemistry, some chemically inspired ansatzes have been proposed by adapting classical chemistry algorithms to run efficiently on quantum circuits [4]. The most notable one is the unitary coupled cluster (UCC) [53] adapted from the coupled cluster (CC) method [54]. The variational UCC method is able to converge when used with multireference initial states. The UCC is usually truncated at the single and double excitations, known as the unitary coupled cluster with all single and double excitations (UCCSD) [53]. In similar spirit to UCCSD, another commonly used ansatz has been proposed in Ref. [55], which considers all single and double excitation gates acting on the reference state without flipping the spin of the excited particles, but where all gates are Givens rotations [55]. We refer to this ansatz as Givens rotations with all single and double excitations (GRSD) in this paper. Moreover, adaptive ansatzes have been presented in Refs. [22,23,56], where the structure of quantum circuits is optimized adaptively. It has been shown that these adaptive ansatzes perform better in terms of both circuit depth and chemical accuracy than circuits that use parameter updates alone. For these problem-specific methods, their performance usually relies upon the choice of initial reference states [57–59], which are often hard to determine.

In this paper, we present a hardware-efficient ansatz for eigensolvers which allows for rapid adjustment of the entanglement to the required amount by making entanglers variational. Our ansatz is thus referred to as the entanglement-variational hardware-efficient ansatz (EHA). We validate its efficiency via numerical comparisons with some widely used VQE ansatzes. By solving benchmark problems in quantum many-body physics and quantum

TABLE I. The full forms of the acronyms frequently used in this paper.

Acronym	Description
<i>Quantum many-body model</i>	
HM	Heisenberg model
TFIM	Transverse field Ising model
BHM	Bose-Hubbard model
<i>Variational quantum eigensolver (VQE) ansatz</i>	
EHA	Entanglement-variational hardware-efficient ansatz
HEA	Hardware-efficient ansatz
HVA	Hamiltonian variational ansatz
HSA	Hardware symmetry-preserving ansatz
GRSD	Givens rotations with all single and double excitations
UCCSD	Unitary coupled cluster with all single and double excitations
ADAPT-VQE	Adaptive derivative-assembled pseudo-Trotter ansatz variational quantum eigensolver

chemistry, our EHA has the following advantages. (1) It is hardware-efficient and can be applied to various kinds of problems, particularly suitable for NISQ devices. (2) In most numerical experiments, EHA can attain a higher level of accuracy than other ansatzes, even compared with problem-specific ansatzes. (3) For different choices of initial reference states and variational parameters, the performance of EHA is more robust as compared to other ansatzes. (4) The variational entangler design enables EHA to quickly adjust the entanglement to the desired amount, which is also the fundamental reason for its superiority.

This paper is organized as follows. In Sec. II, for subsequent comparison, we first introduce several basic models and corresponding ansatzes. Then we present our EHA, and demonstrate its advantages via numerical comparisons with other ansatzes in Sec. III. Section IV concludes the main text of the paper. Several appendixes then follow. Since we utilize many acronyms, for the convenience of the reader, in Table I we summarize the full forms of those frequently used.

## II. PRELIMINARIES

In this paper, we focus on the task of finding ground eigenstates and the corresponding eigenenergies of Hamiltonians in quantum many-body physics and quantum chemistry. In this section, we introduce the models and ansatzes to be used for comparison with our EHA.

### A. Quantum many-body models

For quantum many-body physics, we first consider a one-dimensional chain Heisenberg model (HM) consisting

of  $N$  spins [51,52], whose Hamiltonian reads

$$H_{\text{HM}} = J \sum_{i=1}^{N-1} (\sigma_i^x \sigma_{i+1}^x + \sigma_i^y \sigma_{i+1}^y + \sigma_i^z \sigma_{i+1}^z). \quad (1)$$

Here  $J = 1$  sets the unit of energy; and  $\sigma_i^x$ ,  $\sigma_i^y$ , and  $\sigma_i^z$  denote the Pauli  $X$ ,  $Y$ , and  $Z$  operators acting on the  $i$ th qubit, respectively. The Hamiltonian (1) describes a model of interacting systems that cannot be mapped to free fermions. It supports symmetries, including the conservation of the spin components in all directions, i.e.,  $[H_{\text{HM}}, S_\alpha] = 0$  with  $S_\alpha = (1/2) \sum_i \sigma_i^\alpha$  for  $\alpha = x, y, z$ , as well as the total spin, namely  $[H_{\text{HM}}, S_{\text{tot}}^2] = 0$  with  $S_{\text{tot}}^2 = S_x^2 + S_y^2 + S_z^2$ .

We also consider free fermionic systems described by the transverse field Ising model (TFIM) [51,52], whose Hamiltonian reads

$$H_{\text{TFIM}} = J_z \sum_{i=1}^{N-1} \sigma_i^z \sigma_{i+1}^z + h_x \sum_{i=1}^N \sigma_i^x, \quad (2)$$

where  $J_z$  represents the exchange coupling, and  $h_x$  depicts the strength of the transverse magnetic field. For this Hamiltonian, it is well known that a quantum phase transition occurs at  $J_z = h_x$ , and, at this critical point, the ground state is highly entangled and in a complex form [52].

## B. Hardware-efficient ansatzes

In the NISQ era, VQEs have been proposed for eigensolvers with the hope to demonstrate potential quantum advantages when dealing with large systems which are beyond the power of classical computers.

Given a Hamiltonian  $H$ , when employing VQEs, we first need to design an ansatz to build a PQC  $U(\theta)$  with variational parameters  $\theta$ . Starting from a given initial reference state  $|\psi_0\rangle$ , we use the generated trial state  $|\psi(\theta)\rangle = U(\theta)|\psi_0\rangle$  to approximate the ground state of  $H$ . The variational parameters  $\theta$  are adaptively updated by a classical optimizer via minimizing the expectation of  $H$  at the trial state, which reads

$$C(\theta) = \text{Tr}[HU(\theta)|\psi_0\rangle\langle\psi_0|U^\dagger(\theta)]. \quad (3)$$

To minimize the hardware noise in the NISQ era, HEAs have been widely used for eigensolvers. Three commonly used HEAs are illustrated in Fig. 1, and will be compared with our EHA. The initial reference state of these three HEAs is usually set to be  $\rho_0 = |0\rangle\langle 0|$ . For the circuit in Fig. 1(a), the single-qubit rotations take the form

$$\text{Rot}(\phi, \theta, \omega) = R_z(\omega)R_y(\theta)R_z(\phi), \quad (4)$$

with  $R_z(\phi) = e^{-i\phi Z/2}$  and  $R_y(\theta) = e^{-i\theta Y/2}$ , and the entangling gates are CX gates arranged in a line pattern [42].

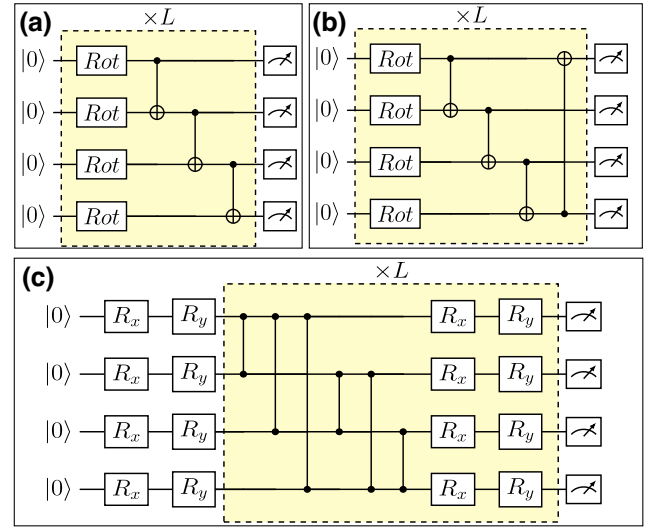


FIG. 1. Quantum circuits for HEAs. (a) CX-line, whose single-qubit modules are  $\text{Rot}$  gates defined in Eq. (4), and the entangling gates are CX gates arranged in a line pattern. (b) CX-ring, whose entangling gates are arranged in a ring pattern. (c) CZ-complete, whose single-qubit modules are  $R_x, R_y$  gates, and the entangling gates are CZ gates arranged in a complete pattern. The yellow shaded circuits are repeated  $L$  times.

Thus, we refer to it as CX-line. The ansatz in Fig. 1(b) is named CX-ring, since its single-qubit modules and entangling gates are the same as those in CX-line, except that the entangling gates are in a ring pattern [41]. For the ansatz in Fig. 1(c), its single-qubit rotations are in the form  $R_y(\theta)R_x(\phi)$  with  $R_x(\phi) = e^{-i\phi X/2}$  [31]. Since its entangling gates are CZ gates arranged in a complete pattern [60], we call it CZ-complete.

## C. Problem-specific ansatzes

The problem-agnostic HEAs often suffer from difficult training issues. In addition, HEAs do not preserve any symmetry in general. In this subsection, we briefly introduce two important problem-specific ansatzes: the Hamiltonian variational ansatz [51] and the hardware symmetry-preserving ansatz [52].

### 1. HVA

Assume the Hamiltonian  $H$  can be decomposed into a sum with a total number of terms  $S$  as

$$H = \sum_{s=1}^S H_s. \quad (5)$$

Then we can construct the HVA in the form

$$U(\theta) = \prod_{l=1}^L \left[ \prod_{s=1}^S \exp(-i\theta_{l,s} H_s) \right]. \quad (6)$$

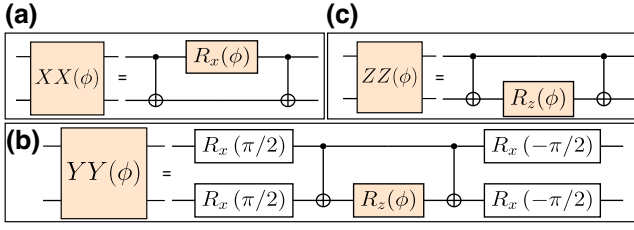


FIG. 2. Hardware-efficient circuits for entangling gates: (a) circuit for  $XX$ ; (b) circuit for  $YY$ ; and (c) circuit for  $ZZ$ .

Specifically, for an  $N$ -qubit HM described by Eq. (1), when the qubit number is even, its Hamiltonian can be decomposed into [51]

$$H_{\text{HM}} = H^{\text{even}} + H^{\text{odd}},$$

with

$$H^{\text{even}} = H_{xx}^{\text{even}} + H_{yy}^{\text{even}} + H_{zz}^{\text{even}},$$

$$H^{\text{odd}} = H_{xx}^{\text{odd}} + H_{yy}^{\text{odd}} + H_{zz}^{\text{odd}},$$

where for  $\alpha = x, y, z$  one has  $H_{\alpha\alpha}^{\text{even}} = \sum_{i=1}^{N/2} \sigma_{2i-1}^{\alpha} \sigma_{2i}^{\alpha}$  and  $H_{\alpha\alpha}^{\text{odd}} = \sum_{i=1}^{N/2-1} \sigma_{2i}^{\alpha} \sigma_{2i+1}^{\alpha}$ . Then  $U_{\text{HM}}(\theta, \phi, \beta, \gamma)$  reads

$$\begin{aligned} U_{\text{HM}}(\theta, \phi, \beta, \gamma) &= \prod_{l=1}^L [G(\gamma_l, H_{xx}^{\text{even}}) G(\gamma_l, H_{yy}^{\text{even}}) G(\beta_l, H_{zz}^{\text{even}}) \\ &\quad \times G(\phi_l, H_{xx}^{\text{odd}}) G(\phi_l, H_{yy}^{\text{odd}}) G(\theta_l, H_{zz}^{\text{odd}})], \end{aligned}$$

with  $G(x, A) = e^{-i(x/2)A}$ .

The whole circuit for  $U_{\text{HM}}(\theta, \phi, \beta, \gamma)$  can be found in Fig. 19 in Appendix A. To implement  $U_{\text{HM}}(\theta, \phi, \beta, \gamma)$ , the entangling operators  $XX(\phi) = e^{-i(\phi/2)(X \otimes X)}$ ,  $YY(\phi) = e^{-i(\phi/2)(Y \otimes Y)}$ , and  $ZZ(\phi) = e^{-i(\phi/2)(Z \otimes Z)}$  are employed, whose circuits are illustrated in Fig. 2.

Note that the initial reference state plays a crucial role in problem-inspired ansatzes [28,29], which is quite different from the case in HEAs. To guarantee the efficiency of HVA for the HM, the initial reference state is chosen to be  $\otimes^{N/2} |\Psi^-\rangle$  with  $|\Psi^-\rangle = (1/\sqrt{2})(|01\rangle - |10\rangle)$ .

As for an  $N$ -qubit TFIM with  $J_z = h_x = -1$  and  $N$  being even, the Hamiltonian  $H_{\text{TFIM}}$  can be decomposed into

$$H_{\text{TFIM}} = - \sum_{i=1}^{N-1} \sigma_i^z \sigma_{i+1}^z - \sum_{i=1}^N \sigma_i^x = H_{zz} + H_x, \quad (7)$$

with  $H_{zz} = - \sum_i \sigma_i^z \sigma_{i+1}^z$  and  $H_x = - \sum_i \sigma_i^x$ . Then the HVA  $U_{\text{TFIM}}(\beta, \gamma)$  reads

$$U_{\text{TFIM}}(\beta, \gamma) = \prod_{l=1}^L \left[ \exp\left(-i\frac{\gamma_l}{2} H_x\right) \exp\left(-i\frac{\beta_l}{2} H_{zz}\right) \right],$$

whose circuit diagram is illustrated in Fig. 21(a) in Appendix A. For the TFIM, the initial reference state is chosen to be  $\otimes^N |+\rangle$  with  $|+\rangle = (1/\sqrt{2})(|0\rangle + |1\rangle)$ .

## 2. HSA

In Ref. [52], an HSA was proposed to improve the performance of eigensolvers by exploiting the symmetries of the Hamiltonian.

To be specific, if the ansatz  $U(\theta)$  satisfies  $[U(\theta), S_z] = 0$ , then it conserves the number of excitations. While if  $[U(\theta), S_{\text{tot}}^2] = 0$ , then it preserves the total spin. To realize HSA, the more complex entangling gate [61]

$$\mathcal{N}(\theta, \phi, \beta) = e^{i(\theta \sigma_1^x \sigma_2^x + \phi \sigma_1^y \sigma_2^y + \beta \sigma_1^z \sigma_2^z)}$$

has been employed. The circuit for realizing  $\mathcal{N}(\theta, \phi, \beta)$  is shown in Fig. 1(b) in Ref. [52] (and see Fig. 20(b) in Appendix A).

As for the HM in Eq. (1), single block circuits for realizing  $S_z$ -conserving and  $S_{\text{tot}}$ -conserving ansatzes are shown in Fig. 1(c) and Fig. 1(d), respectively, in Ref. [52]. For ease of reading, we illustrate the HSA circuit in Fig. 20 in Appendix A. Since the ground state of the Hamiltonian (1) is a global singlet with both total spin  $s = 0$  and spin component  $s_z = 0$ , the initial reference state is chosen to be  $\otimes^{N/2} |\Psi^-\rangle$  to guarantee the preservation of these symmetries in trial states.

The authors in Ref. [52] also generalized the HSA to solve the TFIM, whose circuit is shown in Fig. 7(a) in Ref. [52] (see also Fig. 21(b) in Appendix A). The initial reference state is chosen to be  $\otimes^N |+\rangle$ .

## D. Quantum chemistry models and ansatzes

Solving the low-lying energies of the electrons in molecules has attracted significant attention [4] since it was first introduced [62] in the context of quantum computational chemistry. It is often a starting point for more complex analysis in chemistry, including the calculation of reaction rates, and the determination of molecular geometries and thermodynamic phases, among others [63].

In this paper, we try to find the ground eigenstates and eigenenergies of the electronic Hamiltonian of the  $\text{H}_3^+$  cation, and the HF,  $\text{H}_5$ ,  $\text{BeH}_2$ , and  $\text{LiH}$  molecules. For conciseness, we work in atomic units, where the length unit is 1 Å (1 Å =  $1 \times 10^{-10}$  m), and the energy unit is 1 Hartree (1 Hartree = 27.211 eV). We utilize the second quantized representation to simulate chemical systems on a quantum computer [64]. To do this, we need to select a basis set, which is used to approximate the spin-orbitals of the investigated molecule. A suitably large basis set is crucial for obtaining accurate results. In this paper, we take the Slater-type orbital-3 Gaussians (STO-3G) [65] as the spin-orbital basis for second quantization. Then we utilize the occupation number basis to represent whether a spin-orbital is

occupied. Next we can employ the Jordan-Wigner encoding [66] to map the second quantized fermionic Hamiltonian into a linear combination of Pauli strings, each of which is a product of single-qubit Pauli operators. More details can be found in Ref. [4].

While it is important to understand the whole procedure of how to map electronic structure problems onto a quantum computer, every step from selecting a basis to producing an encoded qubit Hamiltonian can be carried out using a quantum computational chemistry package such as OpenFermion [67] or PennyLane [68]. In this paper, we adopt PennyLane to implement UCCSD and GRSD.

### III. MAIN RESULTS

In this section, we first present our hardware-efficient ansatz having variational entangling gates for eigensolvers. We then compare it with the ansatzes introduced by focusing on models introduced in Sec. II.

#### A. Entanglement-variational hardware-efficient ansatz

Our aim is to design a hardware-efficient ansatz for eigensolvers which can be efficiently applied to solve various kinds of Hamiltonians for different systems.

To approximate target ground states, it is imperative to generate trial states having a matched amount of entanglement. However, there is a lack of freedom to adjust entanglement to the required level in most of the existing HEAs, as their entanglers are fixed. The entanglement can usually be generated within a few layers; however, once the entanglement is in excess of the requirement, it cannot be removed efficiently. The excess entanglement will result in too much expressibility, leading to the phenomenon of BPs, which makes the training extremely difficult and greatly hampers the efficiency of HEAs.

Note that the entanglement is generated through entangling gates. Therefore, to improve the ability of regulating the generated entanglement of HEAs, a natural idea is to make entangling gates tunable with variational parameters. Based on this, we present our entanglement-variational hardware-efficient ansatz as illustrated in Fig. 3.

It is clear that the entanglers

$$U_{\text{ent}}(\boldsymbol{\theta}_{l,i}) = ZZ(\theta_{l,i,3})YY(\theta_{l,i,2})XX(\theta_{l,i,1})$$

are tunable, which is the most significant difference from existing HEAs. Our ansatz is hardware-efficient, since the variational  $XX$ ,  $YY$ , and  $ZZ$  gates can be realized by native single-qubit gates and  $CX$  gates as illustrated in Fig. 2. Moreover, we would like to point out that, since the entanglers  $XX$ ,  $YY$ , and  $ZZ$  are native to the hardware itself in some quantum computers [69], this can further significantly improve the efficiency of our EHA.

Although HVA and HSA also employ variational  $XX$ ,  $YY$ , and  $ZZ$  gates to implement entangling operations, the

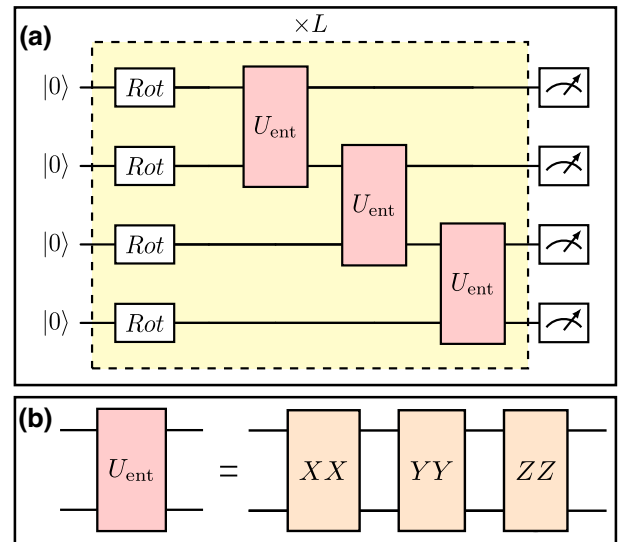


FIG. 3. Quantum circuit for EHA. (a) The circuit consists of  $L$  blocks, and each block is composed of a layer of single-qubit rotational gates defined by Eq. (4) and variational entanglers  $U_{\text{ent}}$  arranged in a line pattern. (b) Each variational entangler  $U_{\text{ent}}$  is composed of  $XX$ ,  $YY$ , and  $ZZ$  gates in series, whose realizations are illustrated in Fig. 2. The variational parameters of the entanglers are (in general) different. The initial reference state is set to be  $\bigotimes^n |0\rangle$ .

principle of their design is rather different from our EHA. There they first decompose the Hamiltonian of a specific problem into components as in Eq. (5), and then design variational circuits to realize each component Hamiltonian as described by Eq. (6). Note that in quantum many-body physics, Hamiltonians are described in terms of Pauli strings. Thus, when realizing the component Hamiltonians, variational gates, e.g.,  $XX$ , naturally appear. Their constructed circuits are problem-specific. However, our EHA is problem-agnostic and can be applied to various problems.

Moreover, it is worth pointing out that for the HM, although the circuits of EHA (Fig. 3), HVA (Fig. 19), and HSA (Fig. 20) appear similar apart from the way the entangling gates are arranged, there is an additional layer of single-qubit rotational gates with each having three variational parameters as described by Eq. (4) for each block. For the TFIM, compared to HVA and HSA (Fig. 21), each block of EHA (Fig. 3) has more degrees of freedom in adjusting the entangling and single-qubit variational gates. It has been demonstrated [70] that, by increasing the number of variational parameters, local minima of the cost function can be transformed into saddle points. Furthermore, it has been shown that gradient descent converges only to minima rather than to saddle points [71]. Thus, the additional degrees of variational parameters in our EHA can help enhance the performance of eigensolvers

compared to HVA and HSA. This will be validated in the following subsections.

We now compare our EHA with the ansatzes introduced in Sec. II in finding the ground states and their energies of Hamiltonians of various kinds of systems. In this paper, the actual ground states and their energies of Hamiltonians are obtained by employing the classical method NumPy [72]. We demonstrate that, as compared with other ansatzes, our EHA can approximate the target ground states with a higher level of accuracy in most cases, and its performance is more robust with respect to different initializations and different initial reference states. In addition, our EHA can quickly adjust the entanglement of trial states to the required amount.

## B. Higher level of accuracy and robustness

### 1. Quantum many-body problems

In the first part of Sec. III B, we focus on finding eigenstates of a 12-qubit HM in Eq. (1) and a 12-qubit TFIM in Eq. (2).

Since two-qubit entangling gates are valuable resources in quantum computing, when comparing the performance of different ansatzes, to be fair, we ensure that they employ roughly the same number of basic two-qubit entangling gates. As an illustration, when solving an  $N$ -qubit HM ( $N$  is even), as shown in Figs. 2 and 3, our EHA utilizes a total number of  $6(N - 1)$  CX gates per block, whereas, for each block, there are  $(N - 1)$  CX gates for CX-line,  $N$  CX gates for CX-ring,  $N(N - 1)/2$  CZ gates for CZ-complete,  $6(N - 1)$  CX gates for HVA, and  $3(N - 1)$  CX gates for HSA. Here, we do not include the CX gates utilized to prepare the initial reference states for HVA and HSA. Thus, if there are  $L$  blocks in our EHA, then the number of blocks should be  $6L$  for CX-line,  $\lceil 6L(N - 1)/N \rceil$  for CX-ring,  $\lceil 12L/N \rceil$  for CZ-complete,  $L$  for HVA, and  $2L$  for HSA. Here,  $\lceil \cdot \rceil$  denotes the roundup function.

As for the initialization of variational parameters, for CZ-complete, we use Gaussian initialization whose mean is 0 and variance is  $1/L$  as mentioned in Ref. [31]; whereas for the other ansatzes, we adopt the uniform distribution  $\mathcal{U}[-\pi, \pi]$ . We employ the Adam optimizer provided by PennyLane for training, and the step size is set to be 0.01 for all ansatzes, unless otherwise stated. Each ansatz is implemented 10 times, and for each realization the initial parameters are drawn according to the assumed distribution. In the following figures, the black dashed line denotes the actual ground-state energy of the considered case, which serves as a baseline for comparison. All the other lines indicate the respective average value of the expectation of the considered Hamiltonian over 10 realizations for different ansatzes. The shaded areas represent the smallest area that includes all the behaviors of the 10 realizations. Here, for simplicity, we do not take into account the impact of limited measurement shots, which is a limiting factor

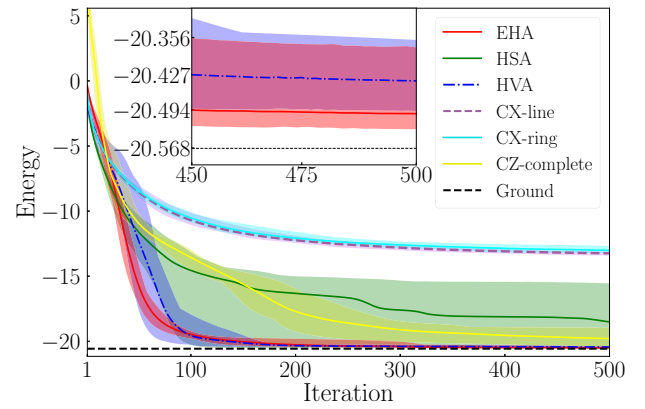


FIG. 4. Comparison of our EHA with other ansatzes for the HM in Eq. (8). The inset illustrates the fine difference between EHA and HVA. Our EHA is superior to other ansatzes in obtaining a lower energy, and its performance is robust with respect to different realizations.

for NISQ devices. We also perform additional experiments under limited shot counts, and the results demonstrate that our EHA has similar advantages to the ideal case (infinite shots) compared to other ansatzes. We illustrate one of the results in Appendix B.

For comparison, we first consider a 12-qubit HM, whose Hamiltonian reads

$$H_{\text{HM}} = \sum_{i=1}^N (\sigma_i^x \sigma_{i+1}^x + \sigma_i^y \sigma_{i+1}^y + \sigma_i^z \sigma_{i+1}^z), \quad (8)$$

with  $N = 12$ . The numbers of blocks in our EHA, CX-line, CX-ring, CZ-complete, HVA, and HSA are 10, 60, 55, 10, 10, and 20, respectively. We illustrate their performance in Fig. 4. From the perspective of the average energy over different realizations, it is clear that our EHA outperforms all the other ansatzes. Among them, the performances of CX-ring and CX-line are very poor. The performance of HSA has an obvious gap with our EHA. In addition, our EHA is robust to different parameter initializations, since all 10 realizations approximately converge to the actual ground-state energy. In contrast, the performance of HSA is very sensitive to parameter initializations.

Next, for the 12-qubit TFIM, we first consider a Hamiltonian which reads

$$H_{\text{TFIM}} = - \sum_{i=1}^{N-1} \sigma_i^z \sigma_{i+1}^z + 3.5 \sum_{i=1}^N \sigma_i^x, \quad (9)$$

with  $N = 12$ . The numbers of blocks in our EHA, CX-line, CX-ring, CZ-complete, HVA, and HSA are 4, 24, 22, 4, 4, and 8, respectively. The results are illustrated in Fig. 5. We find that our EHA outperforms all the other ansatzes, as it can robustly attain a lower energy.

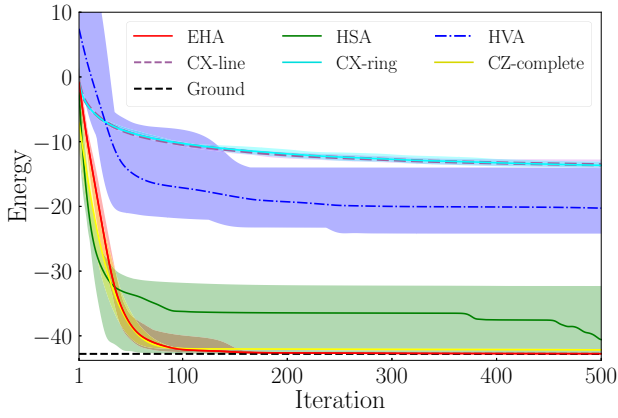


FIG. 5. Comparison of our EHA with other ansatzes for the TFIM in Eq. (9). Our EHA is much better than the other ansatzes, as it can robustly obtain a lower energy.

Recall that HSA is a problem-specific ansatz that is utilized to improve the performance of VQE. However, from Figs. 4 and 5, it is clear that the sample variance of HSA is much larger than for other ansatzes. This implies that its performance relies on different initial parameters. In fact, in the above experiments, it does not always provide a good approximation to the actual solution. However, it does converge to the solution approximately under some initializations. This is demonstrated in Fig. 6, where we plot the best performance of our EHA and HSA among 10 experiments for the HM in Eq. (8) and the TFIM in Eq. (9). We find that from the perspective of the best performance, the problem-specific HSA is slightly better than our EHA. Nevertheless, it is important to note that our ansatz is problem-agnostic, and it is more robust to different realizations.

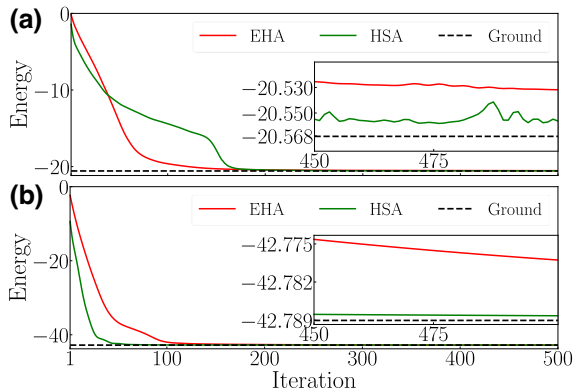


FIG. 6. The best performance of EHA and HSA among 10 experiments for (a) the HM in Eq. (8) and (b) the TFIM in Eq. (9). The insets illustrate their fine differences. HSA is slightly better than our EHA in obtaining a lower energy.

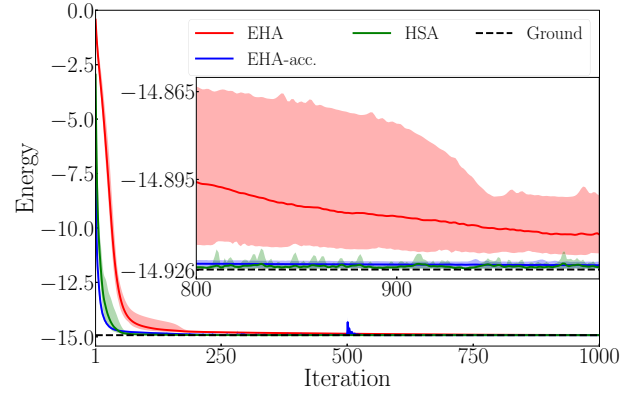


FIG. 7. Comparison between our EHA and HSA for the TFIM in Eq. (10). Although HSA outperforms EHA, the performance of EHA with acceleration is similar to that of HSA.

We then consider the TFIM in Eq. (2) with  $J_z = h_x = -1$ , whose Hamiltonian reads

$$H_{\text{TFIM2}} = - \sum_{i=1}^{11} \sigma_i^z \sigma_{i+1}^z - \sum_{i=1}^{12} \sigma_i^x. \quad (10)$$

Recall that for the Hamiltonian in Eq. (2), a quantum phase transition occurs at  $J_z = h_x$ , and at this critical point, the ground state is highly entangled and in a complex form [52]. We compare our 10 blocks EHA and 20 blocks HSA, and demonstrate the experimental results in Fig. 7. We find that for the TFIM in Eq. (10), HSA converges to the actual ground-state energy closer and faster than our EHA when using a step size of 0.01. To accelerate the convergence rate of EHA, we can increase its step size to 0.05 for the first 500 iterations and keep 0.01 for the rest. The accelerated version of EHA is referred to as EHA-acc. and its experimental results are also demonstrated in Fig. 7. We find that the performance of EHA-acc. is similar to that of HSA.

## 2. Quantum chemistry problems

Now we compare our EHA with chemically inspired ansatzes UCCSD and GRSD by focusing on the HF molecule and  $\text{H}_3^+$  cation. The quantum circuits for UCCSD and GRSD are much more complicated than our EHA. To be specific, from Figs. 2 and 3, the entangling gates in our EHA are all local CX gates that are applied to nearest-neighbor qubits. However, when realizing UCCSD, it has some nonlocal CX gates, while for GRSD, in addition to nonlocal CX gates, it has some T gates. We list the number of all CX gates, nonlocal CX gates, and T gates of UCCSD and GRSD for the HF molecule and  $\text{H}_3^+$  cation in Table IV in Appendix C. Since most current hardware platforms allow only nearest-neighbor connections [73,74], and the use of T gates causes a very high cost [75], our EHA is much easier to realize with current NISQ devices

compared to UCCSD and GRSD. Thus, in the following we focus only on the performance of EHA, UCCSD, and GRSD without assuming that they have roughly the same number of CX gates.

Recall that we adopt PennyLane to simulate UCCSD and GRSD (referred to as ALLSD in PennyLane). For both of them, we start with the Hartree-Fock state [28]. For our EHA, we project the final output states to the feasible state space, which is spanned by the states considering all single and double excitations above the Hartree-Fock state. We show that our EHA is superior to both of them in robustly obtaining a lower energy.

As for the HF molecule, its bond length is set to be 1.1. Our EHA consists of 12 qubits and has 18 blocks. We demonstrate the experimental results in Fig. 8. Here, the black dashed baseline denotes the ground energy of the HF Hamiltonian obtained by second quantization. We find that our EHA can achieve a lower energy on average and its performance is more robust with respect to different realizations compared to UCCSD and GRSD. While for the best performance among 10 realizations, UCCSD and GRSD are slightly superior to our EHA.

As for the  $H_3^+$  cation, we need to modify the cost function, Eq. (3), by adding a penalty term for our EHA. The reason is as follows. On the one hand, the second quantization Hamiltonian of  $H_3^+$  depends only on the spin-orbital basis, and is independent of the number of electrons [65]. On the other hand, in contrast to UCCSD and GRSD, our EHA does not preserve particle numbers. Therefore, if there is no constraint, under EHA the trial states will converge to the ground state of  $H_3$  having three electrons, while  $H_3^+$  has only two electrons.

To address this issue, we can simply add a constraint on the number of electrons by means of a penalty function.

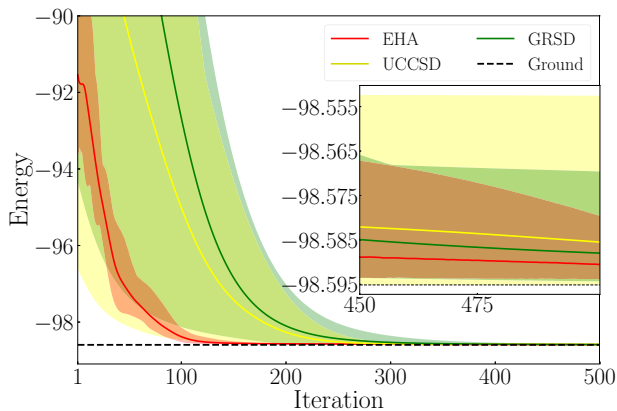


FIG. 8. Comparison of our EHA with UCCSD and GRSD for HF. The black dashed line denotes the ground energy of the HF Hamiltonian obtained by second quantization. Our EHA can robustly achieve a lower average energy as compared to UCCSD and GRSD.

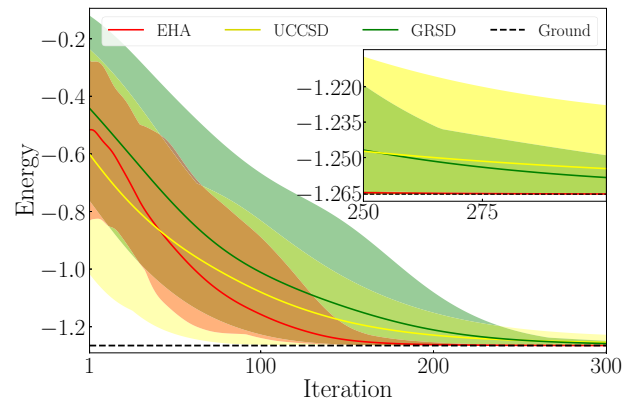


FIG. 9. Comparison of our EHA with UCCSD and GRSD for  $H_3^+$ . The black dashed line denotes the ground energy of the second quantization Hamiltonian of  $H_3^+$ . Our EHA can always achieve the ground energy.

Specifically, we consider the cost function as

$$C(\theta) = \langle \psi(\theta) | H | \psi(\theta) \rangle + \beta [ \langle \psi(\theta) | N | \psi(\theta) \rangle - 2 ]^2. \quad (11)$$

Here,  $H$  is the Hamiltonian of  $H_3^+$ ,  $\beta$  is the penalty hyperparameter, and  $N = \sum_{\alpha} \hat{c}_{\alpha}^{\dagger} \hat{c}_{\alpha}$  denotes the number operator, with  $\hat{c}_{\alpha}^{\dagger}$  and  $\hat{c}_{\alpha}$  being the particle creation and annihilation operators, respectively, and the index  $\alpha$  running over the basis of single particles. Here, for  $H_3^+$ , the bond length is set to be 1.1. Our EHA consists of six qubits and has nine blocks, and the hyperparameter  $\beta = 10$ . The experimental results are shown in Fig. 9. We find that our EHA is much better than UCCSD and GRSD, as EHA can always achieve the ground energy for different realizations.

### C. Ability to quickly adjust entanglement

Recall that, to solve the ground-state problem, it is imperative to generate a quantum state with the matched entanglement. In this subsection, we demonstrate that because of the variational entangler design in our EHA, it can rapidly adjust the entanglement to the required amount during the training process.

For an  $N$ -qubit system state  $\rho$ , denote by  $\rho_i$  the state of the  $i$ th qubit by taking the partial trace over all the other qubits, namely,  $\rho_i = \text{Tr}_{\bar{i}}[\rho]$ , where  $\bar{i}$  denotes the subsystem excluding the  $i$ th qubit. Here, we adopt the average von Neumann entropy

$$S \triangleq -\frac{1}{N} \sum_{i=1}^N \text{Tr}[\rho_i \log(\rho_i)]$$

to be the figure of merit for evaluating the entanglement of quantum state  $\rho$ .



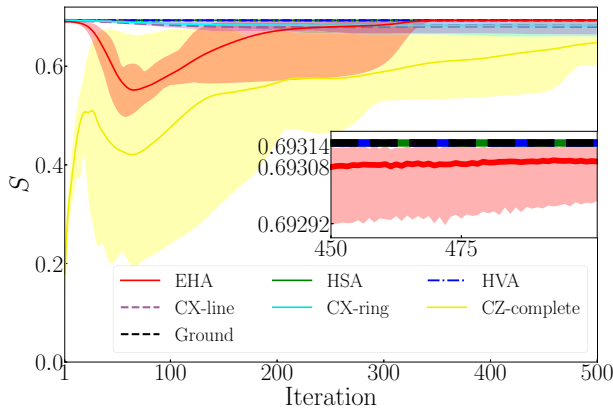


FIG. 10. Entanglement transitions under different ansatzes for the HM in Eq. (8). Our EHA can quickly adjust the entanglement to the desired amount.

For the models already investigated in Sec. III B, we now investigate their entanglement transitions of the generated trial states under different ansatzes during the optimization. In the following figures, the black dashed line denotes the entanglement of the ground state, and the other lines denote the respective average value of the entanglement over 10 realizations under different ansatzes.

For the 12-qubit HM in Eq. (8), we illustrate the entanglement transitions (corresponding to Fig. 4) in Fig. 10. We find that the ground state has a large amount of entanglement. Under HVA and HSA, the entanglement of the generated quantum states stays at the same value as the desired amount during the optimization. This validates that for the problem-specific HVA and HSA, they only explore specific spaces of the unitaries during training. This is the main reason that HVA and HSA usually outperform problem-agnostic HEAs. However, as we mentioned, the performance of HSA and HVA depends heavily on the initial reference states (see Appendix D), which are often hard to determine. For problem-agnostic HEAs, it is clear that our EHA can rapidly adjust the entanglement to the desired level, while the other HEAs cannot. This is due to the variational entangler design in our EHA.

For the 12-qubit TFIM in Eq. (9), we illustrate the entanglement transitions (corresponding to Fig. 5) in Fig. 11. We find that in this case the entanglement of the ground state is low. Under our EHA, the excess entanglement can be quickly removed and adjusted to the desired amount, which is hard to do with other ansatzes. The robustness of the entanglement transitions under different realizations is particularly poor for HSA.

As for the TFIM in Eq. (10), we demonstrate the entanglement transitions under EHA and HSA in Fig. 12. From Figs. 7 and 12, we find that in this case HSA is superior to our EHA, as it can adjust the entanglement to the required level in a much quicker way. However, we note that the

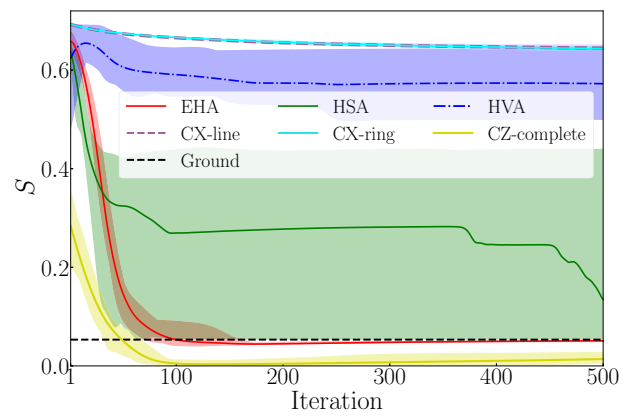


FIG. 11. Entanglement transitions under different ansatzes for the TFIM in Eq. (9). Our EHA is much better than the other ansatzes in adjusting the entanglement to the required amount.

accelerated version of EHA can also tune the entanglement to the required level quickly.

For the  $H_3^+$  cation, the entanglement transitions under EHA, UCCSD, and GRSD (corresponding to Fig. 9) are shown in Fig. 13. Here, we depict only the average value of the entanglement over 10 realizations. We find that, as compared with UCCSD and GRSD, EHA can quickly adjust the entanglement to the desired level.

#### D. The impact of initial reference states

In this subsection, we consider the impact of initial reference states on our EHA. Since the reference state in quantum chemistry problems is typically chosen as the Hartree-Fock state, we are concerned only with quantum many-body systems. Moreover, for problem-specific ansatzes like HSA and HVA, the selection of initial reference states has strict requirements. Taking the HSA as an example, starting from an initial state that violates the symmetry of the Hamiltonian will automatically create a

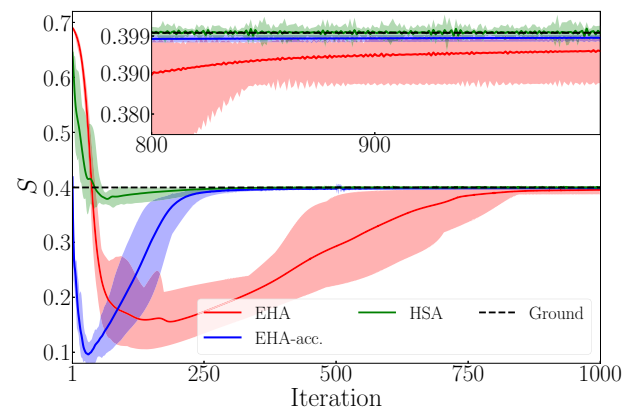


FIG. 12. Entanglement transitions under HSA, EHA, and EHA-acc. for the TFIM in Eq. (10).

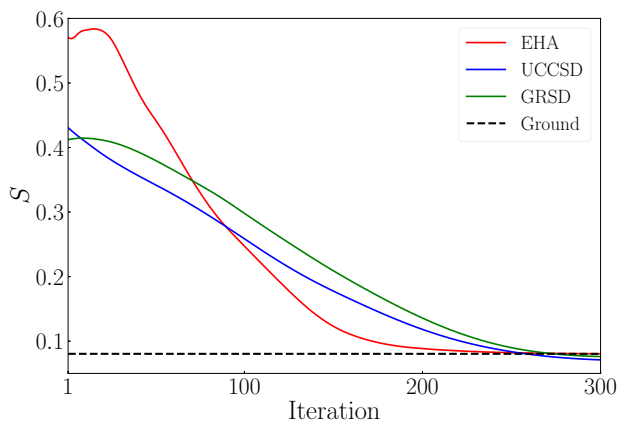


FIG. 13. Entanglement transitions under EHA, UCCSD, and GRSD for  $H_3^+$ .

bias against HSA resulting in poor performance. This has been illustrated in Fig. 23 (in Appendix D). Therefore, we analyze the impact of different initial reference states on ansatzes by comparing the performances of only EHA and HEA. Note that in the above experiments, among the three considered HEAs, the CZ-complete performs best. We now compare EHA with CZ-complete under different initial reference states.

We consider three typical initial reference states:  $\otimes^{12}|0\rangle$ ,  $\otimes^{12}|+\rangle$ , and  $\otimes^6|\Psi^-\rangle$ . The experimental results for the HM in Eq. (8) and the TFIM in Eq. (9) are demonstrated in Figs. 14 and 15, respectively. We find that for both the HM and the TFIM, our EHA is superior to CZ-complete, and the performance of EHA is more robust under different initial reference states. The phenomenon can be explained by checking the corresponding entanglement transitions. As an illustration, we demonstrate the entanglement transitions of the HM (corresponding

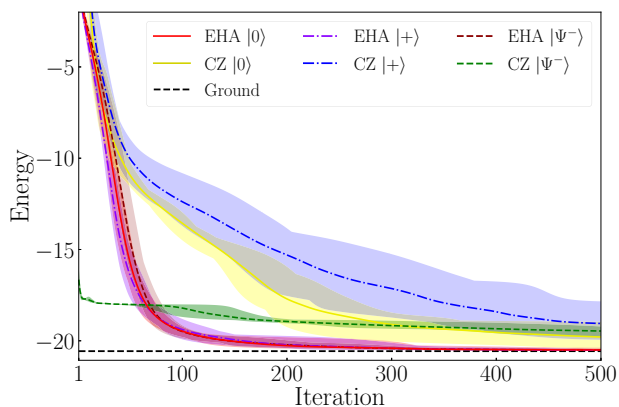


FIG. 14. Comparison between our EHA and CZ-complete under different initial reference states for the HM in Eq. (8). The performance of our EHA is more robust than CZ-complete.

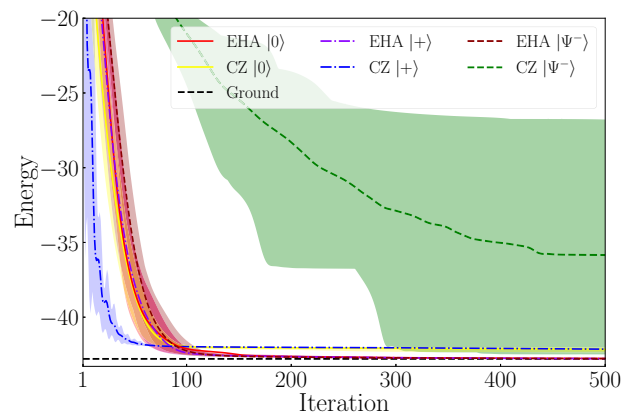


FIG. 15. Comparison between our EHA and CZ-complete under different initial reference states for the TFIM in Eq. (9). The performance of our EHA is more robust than CZ-complete.

to Fig. 14) in Fig. 16. It is clear that, compared to CZ-complete, our EHA can robustly and quickly adjust the entanglement to the desired level under different initial states. This is due to the variational design in EHA, which also makes EHA a strong candidate for quantum computing.

### E. Avoiding BP with reduced-domain initialization

In this subsection, we consider how to train our EHA with relatively large blocks.

As illustrated in Figs. 2 and 3, our EHA utilizes a total number of  $6(N - 1)$  CX gates per block. This makes the expressibility of EHA grow quickly as the number of blocks  $L$  increases. However, it is well known that a too expressive ansatz will result in the phenomenon of

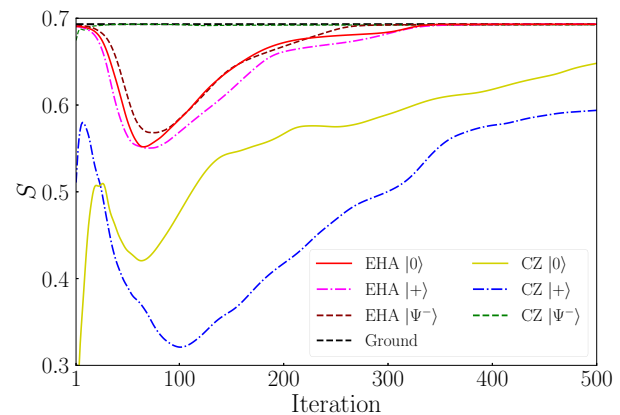


FIG. 16. Entanglement transitions of EHA and CZ-complete under different initial reference states for the HM in Eq. (8). The black dashed line denotes the entanglement of the ground state. Other lines denote the respective average value of the entanglement over 10 realizations. The entanglement transitions of our EHA are more robust than CZ-complete under different initial states.

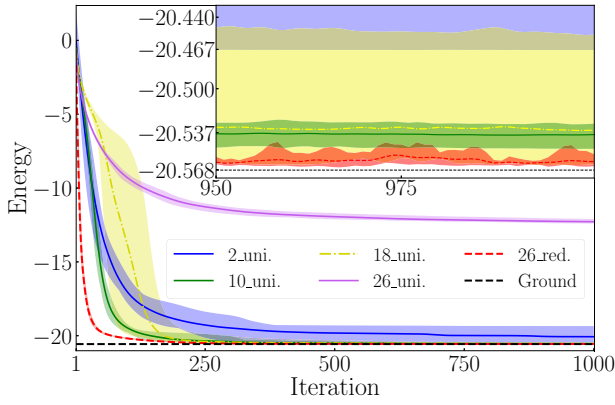


FIG. 17. Performance of EHA under different numbers of blocks and initializations for the HM in Eq. (8). With the reduced-domain initialization, the 26-block circuit can generate quantum states closer to the ground state in a faster way compared to other schemes.

BP, making the training extremely difficult. Therefore, our EHA may suffer from BP when  $L$  is large.

There have been many ways to mitigate the impact of BP [30,31,76–79]. Here, we adopt the reduced-domain method introduced in Ref. [30]. It was stated that to balance the conflict between trainability and expressibility of PQCs, the domain of each variational parameter should be reduced in proportion to  $1/\sqrt{L}$ , where  $L$  denotes the depth of PQC [30]. We demonstrate that the reduced-domain initialization [30] can help train our EHA with relatively large blocks.

We focus on the 12-qubit HM in Eq. (8), and consider four different numbers of blocks, namely,  $L = 2, 10, 18,$  and  $26$ . The experimental settings are the same as those in Sec. III B, except for the initialization.

We first draw the variational parameters according to the uniform distribution  $\mathcal{U}[-\pi, \pi]$ , as we have done in Sec. III B. The numerical results are illustrated in Fig. 17. We find that the 10-block EHA has the best performance among the four considered cases, as it robustly converges to a lower energy. As compared with the 10-block EHA, the two-block EHA is less expressible and cannot obtain better performance, while the 18-block EHA is more expressible but difficult to train [46], which is indicated by the slower convergence rate and larger sample variance. The 26-block EHA is too expressive to be trained. To address the training issue for large blocks of EHA, we

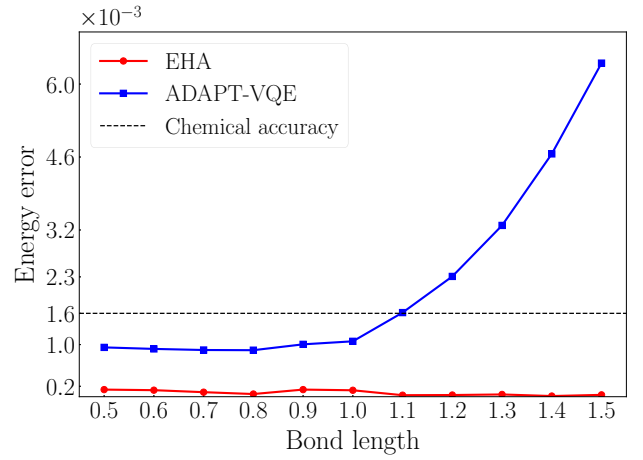


FIG. 18. Ground energy error of EHA and ADAPT-VQE for  $H_5$ . The energy error obtained by ADAPT-VQE exceeds the chemical accuracy and grows quickly when the bond length is larger than 1.1. For our EHA, the energy error stays nearly at the same value as the bond length increases, and is about one-eighth of the chemical accuracy.

leverage the reduced-domain initialization method [30]. Specifically, each variational parameter is drawn according to a reduced uniform distribution  $\mathcal{U}[\pi/2 - 1/\sqrt{L}, \pi/2 + 1/\sqrt{L}]$ . The performance of the 26-block reduced version of EHA is plotted in Fig. 17. We find that with the reduced uniform initialization, the 26-block EHA has a much faster convergence rate, higher level of accuracy, and greater robustness with respect to different realizations, as compared with other cases.

## F. Performance testing

In this subsection, we focus on the performance of our EHA on additional quantum chemistry and quantum many-body models.

We first compare our EHA with an ansatz termed adaptive derivative-assembled pseudo-Trotter ansatz variational quantum eigensolver (ADAPT-VQE), which was proposed in Ref. [22] for molecular simulations. The key idea of ADAPT-VQE is to systematically grow the ansatz by adding fermionic operators one at a time to achieve maximum recovery of the correlation energy at each step. The initial reference state of ADAPT-VQE is also the

TABLE II. Performance of EHA and ADAPT-VQE for different molecules.

Model	Qubits	Blocks	Ground energy	ADAPT-VQE energy	EHA, best	EHA, mean	EHA, STD
BeH <sub>2</sub> (1.1)	14	32	-15.5496	-15.5490	-15.5490	-15.5490	0.0000
LiH(1.11)	12	16	-7.8288	-7.8282	-7.8286	-7.8286	0.0000
HF(1.1)	12	18	-98.5951	-98.5942	-98.5948	-98.5947	0.0000

TABLE III. Performance of EHA for different quantum many-body systems.

Model	Blocks	Ground energy	Energy, best	Energy, mean	Energy, STD	Fidelity, best	Fidelity, mean	Fidelity, STD
HM(8)	14	-13.4997	-13.4994	-13.4993	0.0001	1.0000	1.0000	0.0000
HM(12)	28	-20.5684	-20.5679	-20.5675	0.0002	1.0000	0.9999	0.0000
HM(16)	42	-27.6469	-27.6461	-27.6459	0.0002	0.9999	0.9999	0.0000
TFIM1(8)	6	-20.5018	-20.5018	-20.5015	0.0004	1.0000	1.0000	0.0000
TFIM1(12)	6	-42.7890	-42.7889	-42.7880	0.0010	1.0000	1.0000	0.0000
TFIM1(16)	8	-57.0763	-57.0760	-57.0759	0.0002	1.0000	1.0000	0.0000
TFIM2(8)	8	-9.8380	-9.8378	-9.8376	0.0002	1.0000	0.9999	0.0000
TFIM2(12)	12	-14.9260	-14.9257	-14.9255	0.0002	1.0000	0.9999	0.0000
TFIM2(16)	20	-20.0164	-20.0160	-20.0156	0.0003	0.9999	0.9999	0.0000
BHM(8)	12	0.0000	0.0001	0.0002	0.0001	1.0000	1.0000	0.0000
BHM(16)	20	0.0000	0.0001	0.0002	0.0001	1.0000	1.0000	0.0000

Hartree-Fock state, and the operator pool includes all single and double excitation operators acting on the reference state without flipping the spin of the excited particles. We list the number of all CX gates, nonlocal CX gates, and T gates of ADAPT-VQE for different molecules in Table IV (in Appendix C). It has been shown that ADAPT-VQE outperforms UCC in terms of both circuit depth and chemical accuracy [22].

For all molecules, the ADAPT-VQE results in this paper are obtained by PennyLane, with the termination condition being gradient less than  $10^{-3}$ , whereas, for our EHA, we find that for all experiments, the gradient is never below  $10^{-3}$  before the end of training. This implies that the gradient of EHA is larger than that of ADAPT-VQE before the end of the optimization. Moreover, for all molecules, we have checked that the spin and particle number of the solutions obtained by both ADAPT-VQE and EHA are the same as those of the actual states.

We first consider solving the ground state of  $H_5$  at different bond lengths. Here, we consider the target ground state with  $s_z = 1/2$ . Our EHA consists of 10 qubits,  $L = 38$  blocks, and the initial parameters are drawn from a reduced uniform distribution  $\mathcal{U}[\pi/2 - 1/\sqrt{L}, \pi/2 + 1/\sqrt{L}]$ . To guarantee the obtained state having  $s_z = 1/2$ , similar to what we have done in dealing with  $H_3^+$ , we add an  $S_z$

penalty term (with the hyperparameter being 100) in the cost function in our EHA. We perform 2000 iterations, with the step size being 0.1 for the first 500 iterations, and 0.001 for the last 1500 iterations. We take the minimum energy during the training process as the approximate solution of the ground energy. We illustrate the ground energy error in Fig. 18. We find that when the bond length is larger than 1.1, the ground energy error obtained by ADAPT-VQE exceeds the chemical accuracy ( $1.6 \times 10^{-3}$ ) [80] and grows quickly as the bond length increases, whereas, for our EHA, the energy error remains nearly constant as the bond length increases, and is lower than that for ADAPT-VQE. Specifically, the ground energy error can maintain about one-eighth of the chemical accuracy for bond length ranging from 0.5 to 1.5.

We now apply our EHA and ADAPT-VQE to other molecules. For our EHA we perform at most 3000 iterations, and for different molecules the step size schedules are illustrated in Table V (in Appendix E). The results are demonstrated in Table II. The first column lists the molecules with the bond length in parentheses, the second column shows the number of qubits needed after second quantization of the molecules, and the third column lists the blocks of our EHA. We also list the best value, mean value, and the standard deviation (STD) of the energy

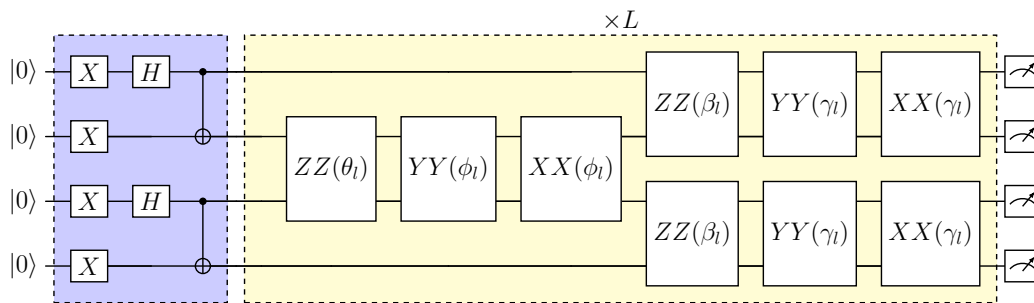


FIG. 19. The HVA circuit for the HM in Eq. (1). In HVA, the parameters of the entanglers are correlated.

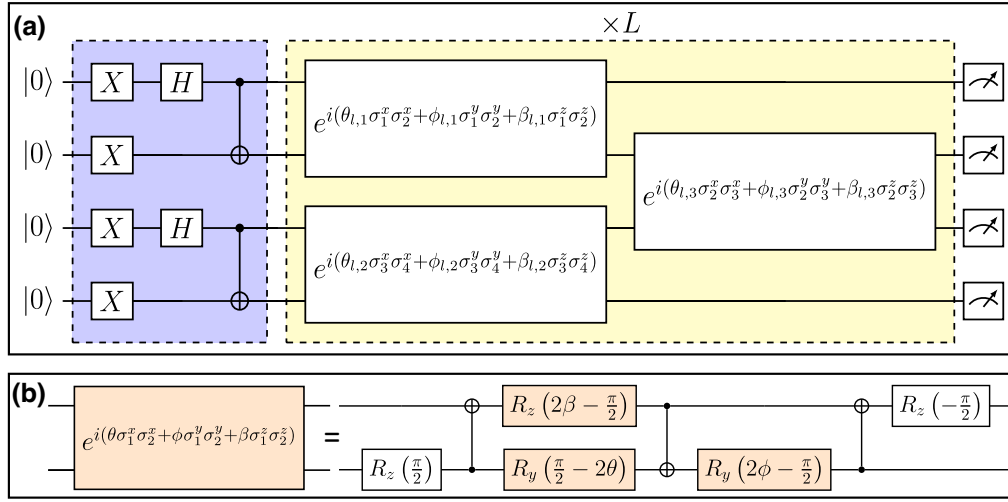


FIG. 20. The HSA circuit for the HM in Eq. (1). (a) The architecture of HSA. (b) Circuit for realizing the entangler  $e^{i(\theta\sigma_1^x\sigma_2^x + \phi\sigma_1^y\sigma_2^y + \beta\sigma_1^z\sigma_2^z)}$  used in HSA.

obtained by our EHA in Table II. It is clear that our EHA outperforms ADPT-VQE and has standard deviation less than  $5 \times 10^{-5}$ .

We further apply our EHA on other quantum many-body systems, where their corresponding step size schedules are illustrated in Table V (in Appendix E). We demonstrate the results in Table III. The first column lists the models with the number of qubits in parentheses, where the HM, TFIM1, and TFIM2 are described by Eqs. (8), (9), and (10), respectively. Here, BHM denotes the Bose-Hubbard model [81] in a chain lattice, whose Hamiltonian reads

$$H = - \left( \sum_{i=1}^{N-1} \hat{b}_i^\dagger \hat{b}_{i+1} + \text{H.c.} \right) + 7 \sum_{i=1}^N \hat{n}_i (\hat{n}_i - 1), \quad (12)$$

where  $\hat{b}_i^\dagger$  and  $\hat{b}_i$  denote the bosonic creation and annihilation operators on site  $i$ , respectively, and  $\hat{n}_i = \hat{b}_i^\dagger \hat{b}_i$  denotes the number operator of site  $i$ . For the BHM, we can use binary bosonic mapping [82] to transform the Hamiltonian in Eq. (12) into the form of a linear combination of Pauli strings, which is done by utilizing PennyLane in this paper. The number of blocks in our EHA is listed in the second column. In Table III, we list the best value, mean value, and the standard deviation of the energy and fidelity obtained by our EHA. We find that for all cases, our EHA can attain the ground energy with a very high level of accuracy. In the best case, the ground energy error is less than  $1 \times 10^{-3}$ , and on average the ground energy error is less than the chemical accuracy of  $1.6 \times 10^{-3}$ . Moreover, the standard deviation is very small, which is at most  $1 \times 10^{-3}$ . The fidelity with the ground state is no smaller

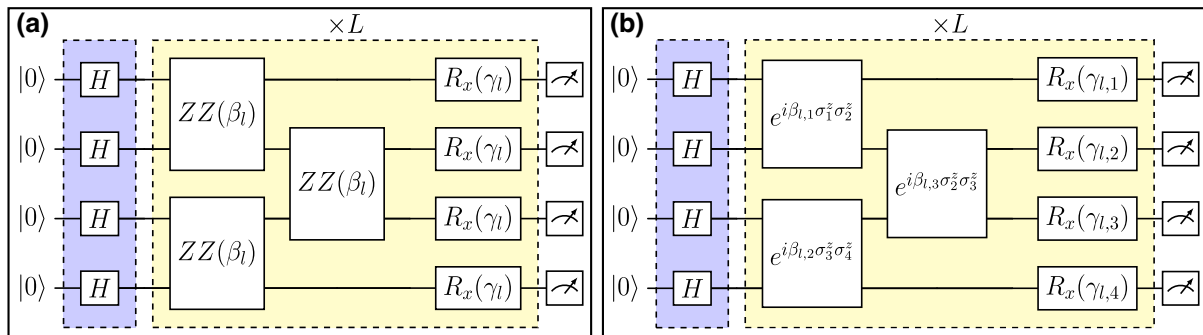


FIG. 21. The HVA and HSA circuits for the TFIM in Eq. (7). (a) The HVA circuit. In each block, there are only two variational parameters, one for the single-qubit rotational gates and the other for the entanglers. (b) The HSA circuit. The gates have different parameters in general. The entangler  $e^{i\beta\sigma_1^x\sigma_2^x}$  can be realized by setting  $\theta = 0$  and  $\phi = 0$  in Fig. 20(b).

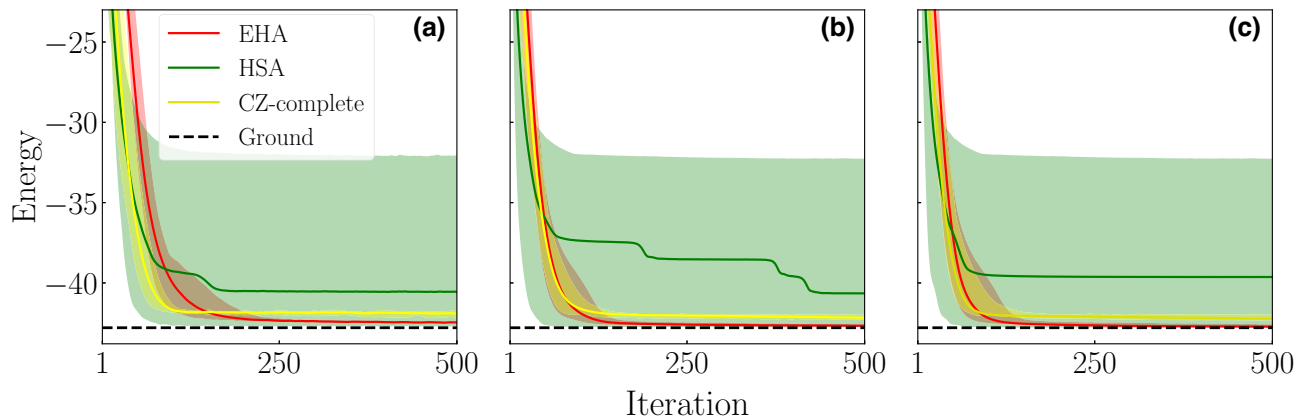


FIG. 22. Performance of EHA, HSA, and CZ-complete under different numbers of measurement shots for the TFIM in Eq. (9). (a) Number of shots is 100. (b) Number of shots is 1000. (c) Number of shots is 5000.

than 99.99% on average, and the standard deviation is lower than  $5 \times 10^{-5}$ .

#### IV. CONCLUSION

In this paper, we propose an efficient hardware-efficient ansatz, EHA, for eigensolvers, in which the entanglers are designed to be variational rather than fixed. This entanglement-variational design allows the circuit to rapidly adjust the entanglement of the generated trial states to the required amount, and in turn greatly enhance the performance. We have demonstrated that our EHA can find approximate solutions for eigensolvers with a very high level of accuracy, and its performance is robust to choices of initial reference states and different realizations. We believe that our EHA is particularly suitable for the NISQ era and will generate wide impact on developing algorithms with potential quantum advantages for various practical applications.

#### ACKNOWLEDGMENTS

B.Q. acknowledges the support of the National Natural Science Foundation of China (No. 61773370), and D.D. acknowledges the support of the Australian Research Council Future Fellowship funding scheme under Project FT220100656.

#### APPENDIX A: CIRCUITS OF PROBLEM-SPECIFIC ANSATZES

For completeness, in Figs. 19, 20, and 21 we illustrate the HVA and HSA circuits for the HM in Eq. (1) and the TFIM in Eq. (7).

#### APPENDIX B: LIMITED MEASUREMENT SHOTS

We consider the practical case where the measurement shots are limited when evaluating the expectation of the

Hamiltonian with respect to the output states of the circuits. We take the TFIM in Eq. (9) as an illustration. Here, we only compare the performance of three typical ansatzes: CZ-complete, HSA, and our EHA. The experimental settings are the same as those in Fig. 5, except for the number of measurement shots. For the ideal case in Fig. 5, the shots are essentially infinite. Here, we consider three different numbers of shots to evaluate the expectation of the Hamiltonian, namely, 100, 1000, and 5000. The experimental results are demonstrated in Fig. 22. It is clear that our EHA outperforms HSA and CZ-complete.

#### APPENDIX C: RESOURCES FOR CHEMICALLY INSPIRED ANSATZES

The resources for different chemically inspired ansatzes are shown in Table IV, where, for the  $H_5$  molecule, (\*) represents all bond lengths ranging from 0.5 to 1.5 with a step size of 0.1 (see Fig. 18).

#### APPENDIX D: THE IMPACT OF INITIAL REFERENCE STATES FOR HSA

From Fig. 23(a), we find that, for the HM, under the reference states  $\otimes^{12}|+\rangle$  and  $\otimes^{12}|0\rangle$ , HSA cannot converge

TABLE IV. Resources for different chemically inspired ansatzes.

Ansatz	Molecule	All CX gates	Nonlocal CX gates	T gates
UCCSD	$H_3^+(1.1)$	272	32	0
UCCSD	HF(1.1)	2400	320	0
GRSD	$H_3^+(1.1)$	64	45	16
GRSD	HF(1.1)	370	272	40
ADAPT-VQE	$H_5^*$	306	246	24
ADAPT-VQE	BeH <sub>2</sub> (1.1)	446	342	24
ADAPT-VQE	LiH(1.11)	366	283	32
ADAPT-VQE	HF(1.1)	152	109	24

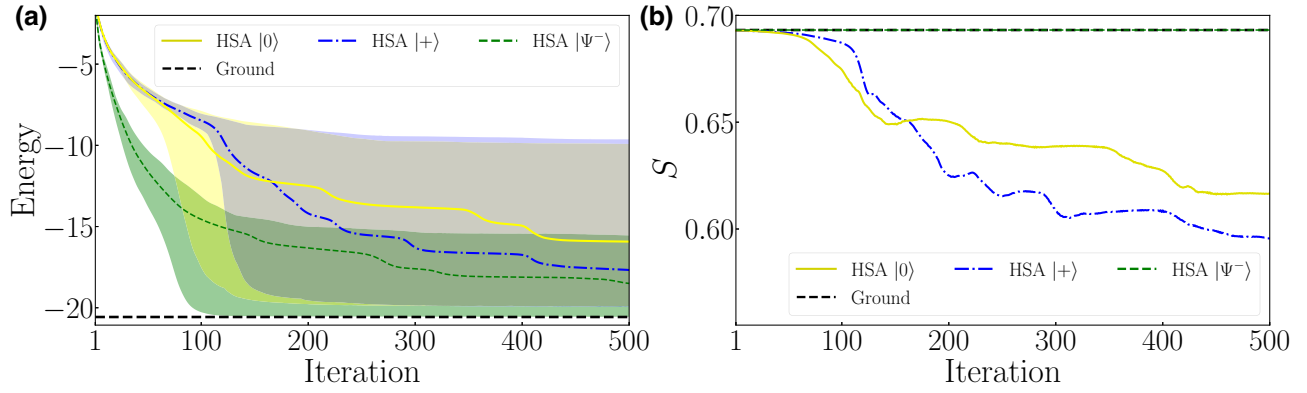


FIG. 23. Performance of HSA under different initial reference states for the HM in Eq. (8). (a) The black dashed line denotes the actual ground-state energy, and all the other lines indicate the respective average value of the energy over 10 realizations under different initial reference states. The shaded areas represent the smallest area that includes all the behaviors of the 10 realizations. (b) The black dashed line denotes the actual entanglement of the ground state, and all the other lines indicate the respective average value of the entanglement over 10 experiments under different reference states.

to the ground state. This validates that the performance of the problem-specific HSA is largely dependent on the reference state. This phenomenon can be explained by checking the corresponding entanglement transitions in Fig. 23(b). We find that, once the initial state is changed to  $\otimes^{12}|+\rangle$  or  $\otimes^{12}|0\rangle$ , HSA cannot maintain the same

amount of entanglement as the ground state, in turn resulting in poor performance.

## APPENDIX E: STEP SIZE SCHEDULE

The step size schedule for the various different models is shown in Table V.

TABLE V. Step size schedule for different models.

Model	Step size	Iteration steps
BeH <sub>2</sub> (1.1)	0.01	1000
	0.005	2000
LiH(1.11)	0.01	1000
	0.005	1000
HF(1.1)	0.01	1000
HM(8)	0.01	1000
HM(12)	0.005	1000
	0.001	1000
	0.0005	2000
	0.005	3000
HM(16)	0.001	2000
	0.0005	2000
	0.01	2000
TFIM1(8)	0.01	2000
TFIM1(12)	0.01	4000
TFIM1(16)	0.01	4000
TFIM2(8)	0.05	500
	0.02	1000
TFIM2(12)	0.02	1500
	0.01	2000
TFIM2(16)	0.02	1000
	0.01	4000
BHM(8)	0.01	1000
BHM(16)	0.01	500
	0.005	500

- [1] Hsin-Yuan Huang, Richard Kueng, Giacomo Torlai, Victor V. Albert, and John Preskill, Provably efficient machine learning for quantum many-body problems, *Science* **377**, eabk3333 (2022).
- [2] I. Stetcu, A. Baroni, and J. Carlson, Variational approaches to constructing the many-body nuclear ground state for quantum computing, *Phys. Rev. C* **105**, 064308 (2022).
- [3] Alan Morningstar, Markus Hauru, Jackson Beall, Martin Ganahl, Adam G. M. Lewis, Vedika Khemani, and Guifre Vidal, Simulation of Quantum Many-Body Dynamics with Tensor Processing Units: Floquet Prethermalization, *PRX Quantum* **3**, 020331 (2022).
- [4] Sam McArdle, Suguru Endo, Alán Aspuru-Guzik, Simon C. Benjamin, and Xiao Yuan, Quantum computational chemistry, *Rev. Mod. Phys.* **92**, 015003 (2020).
- [5] Vincent E. Elfving, Marta Millaruelo, José A. Gámez, and Christian Gogolin, Simulating quantum chemistry in the seniority-zero space on qubit-based quantum computers, *Phys. Rev. A* **103**, 032605 (2021).
- [6] Changsu Cao, Jiaqi Hu, Wengang Zhang, Xusheng Xu, Dechin Chen, Fan Yu, Jun Li, Han-Shi Hu, Dingshun Lv, and Man-Hong Yung, Progress toward larger molecular simulation on a quantum computer: Simulating a system with up to 28 qubits accelerated by point-group symmetry, *Phys. Rev. A* **105**, 062452 (2022).
- [7] Bela Bauer, Sergey Bravyi, Mario Motta, and Garnet Kin-Lic Chan, Quantum algorithms for quantum chemistry

- and quantum materials science, *Chem. Rev.* **120**, 12685 (2020).
- [8] He Ma, Marco Govoni, and Giulia Galli, Quantum simulations of materials on near-term quantum computers, *npj Comput. Mater.* **6**, 85 (2020).
- [9] Lindsay Bassman, Miroslav Urbanek, Mekena Metcalf, Jonathan Carter, Alexander F. Kemper, and Wibe A. de Jong, Simulating quantum materials with digital quantum computers, *Quantum Sci. Technol.* **6**, 043002 (2021).
- [10] Daniel J. Egger, Claudio Gambella, Jakub Marecek, Scott McFaddin, Martin Mevissen, Rudy Raymond, Andrea Simonetto, Stefan Woerner, and Elena Yndurain, Quantum computing for finance: State-of-the-art and future prospects, *IEEE Trans. Quantum Eng.* **1**, 3101724 (2020).
- [11] M. Cerezo, Guillaume Verdon, Hsin-Yuan Huang, Lukasz Cincio, and Patrick J. Coles, Challenges and opportunities in quantum machine learning, *Nat. Comput. Sci.* **2**, 567 (2022).
- [12] John Preskill, Quantum computing in the NISQ era and beyond, *Quantum* **2**, 79 (2018).
- [13] Kishor Bharti, Alba Cervera-Lierta, Thi Ha Kyaw, Tobias Haug, Sumner Alperin-Lea, Abhinav Anand, Matthias Degroote, Hermanni Heimonen, Jakob S. Kottmann, Tim Menke, Wai-Keong Mok, Sukin Sim, Leong-Chuan Kwek, and Alán Aspuru-Guzik, Noisy intermediate-scale quantum algorithms, *Rev. Mod. Phys.* **94**, 015004 (2022).
- [14] Kishor Bharti, Tobias Haug, Vlatko Vedral, and Leong-Chuan Kwek, Noisy intermediate-scale quantum algorithm for semidefinite programming, *Phys. Rev. A* **105**, 052445 (2022).
- [15] Alberto Peruzzo, Jarrod McClean, Peter Shadbolt, Man-Hong Yung, Xiao-Qi Zhou, Peter J. Love, Alán Aspuru-Guzik, and Jeremy L. O'Brien, A variational eigenvalue solver on a photonic quantum processor, *Nat. Commun.* **5**, 4213 (2014).
- [16] M. Cerezo, Andrew Arrasmith, Ryan Babbush, Simon C. Benjamin, Suguru Endo, Keisuke Fujii, Jarrod R. McClean, Kosuke Mitarai, Xiao Yuan, Lukasz Cincio, and Patrick J. Coles, Variational quantum algorithms, *Nat. Rev. Phys.* **3**, 625 (2021).
- [17] Jules Tilly, Hongxiang Chen, Shuxiang Cao, Dario Picozzi, Kanav Setia, Ying Li, Edward Grant, Leonard Wossnig, Ivan Rungger, George H. Booth, and Jonathan Tennyson, The variational quantum eigensolver: A review of methods and best practices, *Phys. Rep.* **986**, 1 (2022).
- [18] Joris Kattemölle and Jasper van Wezel, Variational quantum eigensolver for the Heisenberg antiferromagnet on the kagome lattice, *Phys. Rev. B* **106**, 214429 (2022).
- [19] Andy C. Y. Li, M. Sohaib Alam, Thomas Iadecola, Ammar Jahin, Joshua Job, Doga Murat Kurkcuoglu, Richard Li, Peter P. Orth, A. Barış Özgüler, Gabriel N. Perdue, and Norm M. Tubman, Benchmarking variational quantum eigensolvers for the square-octagon-lattice Kitaev model, *Phys. Rev. Res.* **5**, 033071 (2023).
- [20] Adam Callison and Nicholas Chancellor, Hybrid quantum-classical algorithms in the noisy intermediate-scale quantum era and beyond, *Phys. Rev. A* **106**, 010101 (2022).
- [21] Mateusz Ostaszewski, Edward Grant, and Marcello Benedetti, Structure optimization for parameterized quantum circuits, *Quantum* **5**, 391 (2021).
- [22] Harper R. Grimsley, Sophia E. Economou, Edwin Barnes, and Nicholas J. Mayhall, An adaptive variational algorithm for exact molecular simulations on a quantum computer, *Nat. Commun.* **10**, 3007 (2019).
- [23] Ho Lun Tang, V. O. Shkolnikov, George S. Barron, Harper R. Grimsley, Nicholas J. Mayhall, Edwin Barnes, and Sophia E. Economou, Qubit-ADAPT-VQE: An Adaptive Algorithm for Constructing Hardware-Efficient Ansatzes on a Quantum Processor, *PRX Quantum* **2**, 020310 (2021).
- [24] Mateusz Ostaszewski, Lea M. Trenkwalder, Wojciech Masarczyk, Eleanor Scerri, and Vedran Dunjko, Reinforcement learning for optimization of variational quantum circuit architectures, *Adv. Neural Inf. Process. Syst.* **34**, 18182 (2021).
- [25] Yuxuan Du, Tao Huang, Shan You, Min-Hsiu Hsieh, and Dacheng Tao, Quantum circuit architecture search for variational quantum algorithms, *npj Quantum Inf.* **8**, 62 (2022).
- [26] Li Ding and Lee Spector, in *Proceedings of the Genetic and Evolutionary Computation Conference Companion* (Association for Computing Machinery, New York, 2022), p. 2190.
- [27] Harper R. Grimsley, George S. Barron, Edwin Barnes, Sophia E. Economou, and Nicholas J. Mayhall, Adaptive, problem-tailored variational quantum eigensolver mitigates rough parameter landscapes and barren plateaus, *npj Quantum Inf.* **9**, 19 (2023).
- [28] Google AI Quantum and Collaborators, Hartree-Fock on a superconducting qubit quantum computer, *Science* **369**, 1084 (2020).
- [29] Chris Cade, Lana Mineh, Ashley Montanaro, and Stasja Stanisic, Strategies for solving the Fermi-Hubbard model on near-term quantum computers, *Phys. Rev. B* **102**, 235122 (2020).
- [30] Yabo Wang, Bo Qi, and Chris Ferrie, and Daoyi Dong, Trainability enhancement of parameterized quantum circuits via reduced-domain parameter initialization, [arXiv:2302.06858](https://arxiv.org/abs/2302.06858).
- [31] Kaining Zhang, Liu Liu, Min-Hsiu Hsieh, and Dacheng Tao, Escaping from the barren plateau via Gaussian initializations in deep variational quantum circuits, *Adv. Neural Inf. Process. Syst.* **35**, 18612 (2022).
- [32] James Stokes, Josh Izaac, Nathan Killoran, and Giuseppe Carleo, Quantum natural gradient, *Quantum* **4**, 269 (2020).
- [33] Alicia B. Magann, Kenneth M. Rudinger, Matthew D. Grace, and Mohan Sarovar, Feedback-Based Quantum Optimization, *Phys. Rev. Lett.* **129**, 250502 (2022).
- [34] Shi-Xin Zhang, Zhou-Quan Wan, Chee-Kong Lee, Chang-Yu Hsieh, Shengyu Zhang, and Hong Yao, Variational Quantum-Neural Hybrid Eigensolver, *Phys. Rev. Lett.* **128**, 120502 (2022).
- [35] Nicholas H. Stair and Francesco A. Evangelista, Simulating Many-Body Systems with a Projective Quantum Eigensolver, *PRX Quantum* **2**, 030301 (2021).
- [36] Alba Cervera-Lierta, Jakob S. Kottmann, and Alán Aspuru-Guzik, Meta-variational Quantum Eigensolver: Learning Energy Profiles of Parameterized Hamiltonians for Quantum Simulation, *PRX Quantum* **2**, 020329 (2021).
- [37] Keisuke Fujii, Kaoru Mizuta, Hiroshi Ueda, Kosuke Mitarai, Wataru Mizukami, and Yuya O. Nakagawa, Deep



- Variational Quantum Eigensolver: A Divide-and-Conquer Method for Solving a Larger Problem with Smaller Size Quantum Computers, *PRX Quantum* **3**, 010346 (2022).
- [38] Tobias Haug, Kishor Bharti, and M. S. Kim, Capacity and Quantum Geometry of Parametrized Quantum Circuits, *PRX Quantum* **2**, 040309 (2021).
- [39] Sukin Sim, Peter D. Johnson, and Alán Aspuru-Guzik, Expressibility and entangling capability of parameterized quantum circuits for hybrid quantum-classical algorithms, *Adv. Quantum Technol.* **2**, 1900070 (2019).
- [40] Abhinav Kandala, Antonio Mezzacapo, Kristan Temme, Maika Takita, Markus Brink, Jerry M. Chow, and Jay M. Gambetta, Hardware-efficient variational quantum eigensolver for small molecules and quantum magnets, *Nature* **549**, 242 (2017).
- [41] Maria Schuld, Alex Bocharov, Krysta M. Svore, and Nathan Wiebe, Circuit-centric quantum classifiers, *Phys. Rev. A* **101**, 032308 (2020).
- [42] Boy Choy and David J. Wales, Molecular energy landscapes of hardware-efficient ansätze in quantum computing, *J. Chem. Theory Comput.* **19**, 1197 (2023).
- [43] Lennart Bittel and Martin Kliesch, Training Variational Quantum Algorithms is NP-Hard, *Phys. Rev. Lett.* **127**, 120502 (2021).
- [44] Eric R. Anschuetz and Bobak T. Kiani, Quantum variational algorithms are swamped with traps, *Nat. Commun.* **13**, 7760 (2022).
- [45] Jarrod R. McClean, Sergio Boixo, Vadim N. Smelyanskiy, Ryan Babbush, and Hartmut Neven, Barren plateaus in quantum neural network training landscapes, *Nat. Commun.* **9**, 4812 (2018).
- [46] Zoë Holmes, Kunal Sharma, M. Cerezo, and Patrick J. Coles, Connecting Ansatz Expressibility to Gradient Magnitudes and Barren Plateaus, *PRX Quantum* **3**, 010313 (2022).
- [47] Yanzhu Chen, Linghua Zhu, Nicholas J. Mayhall, Edwin Barnes, and Sophia E. Economou, in *Quantum 2.0* (Optica Publishing Group, Boston, 2022), p. QM4A–2.
- [48] Andreas J. C. Woitzik, Panagiotis Kl. Barkoutsos, Filip Wudarski, Andreas Buchleitner, and Ivano Tavernelli, Entanglement production and convergence properties of the variational quantum eigensolver, *Phys. Rev. A* **102**, 042402 (2020).
- [49] Carlos Ortiz Marrero, Mária Kieferová, and Nathan Wiebe, Entanglement-Induced Barren Plateaus, *PRX Quantum* **2**, 040316 (2021).
- [50] Lorenzo Leone, Salvatore F. E. Oliviero, Lukasz Cincio, and M. Cerezo, On the practical usefulness of the Hardware Efficient Ansatz, [arXiv:2211.01477](https://arxiv.org/abs/2211.01477).
- [51] Roeland Wiersema, Cunlu Zhou, Yvette de Sereville, Juan Felipe Carrasquilla, Yong Baek Kim, and Henry Yuen, Exploring Entanglement and Optimization within the Hamiltonian Variational Ansatz, *PRX Quantum* **1**, 020319 (2020).
- [52] Chufan Lyu, Xusheng Xu, Man-Hong Yung, and Abolfazl Bayat, Symmetry enhanced variational quantum spin eigensolver, *Quantum* **7**, 899 (2023).
- [53] Jonathan Romero, Ryan Babbush, Jarrod R. McClean, Cornelius Hempel, Peter J. Love, and Alán Aspuru-Guzik, Strategies for quantum computing molecular energies using the unitary coupled cluster ansatz, *Quantum Sci. Technol.* **4**, 014008 (2018).
- [54] Rodney J. Bartlett and Monika Musiał, Coupled-cluster theory in quantum chemistry, *Rev. Mod. Phys.* **79**, 291 (2007).
- [55] Juan Miguel Arrazola, Olivia Di Matteo, Nicolás Quesada, Soran Jahangiri, Alain Delgado, and Nathan Killoran, Universal quantum circuits for quantum chemistry, *Quantum* **6**, 742 (2022).
- [56] Roland C. Farrell, Marc Illa, Anthony N. Ciavarella, and Martin J. Savage, Scalable circuits for preparing ground states on digital quantum computers: The Schwinger model vacuum on 100 qubits, [arXiv:2308.04481](https://arxiv.org/abs/2308.04481).
- [57] Zhenyu Cai, Resource estimation for quantum variational simulations of the Hubbard model, *Phys. Rev. Appl.* **14**, 014059 (2020).
- [58] Márten Skogh, Oskar Leinonen, Phalgun Lolur, and Martin Rahm, Accelerating variational quantum eigensolver convergence using parameter transfer, *Electronic Structure* **5**, 035002 (2023).
- [59] Manpreet Singh Jattana, Fengping Jin, Hans De Raedt, and Kristel Michiels, Improved variational quantum eigensolver via quasidynamical evolution, *Phys. Rev. Appl.* **19**, 024047 (2023).
- [60] Joonho Kim, Jaedeok Kim, and Dario Rosa, Universal effectiveness of high-depth circuits in variational eigenproblems, *Phys. Rev. Res.* **3**, 023203 (2021).
- [61] Farrokh Vatan and Colin Williams, Optimal quantum circuits for general two-qubit gates, *Phys. Rev. A* **69**, 032315 (2004).
- [62] Alán Aspuru-Guzik, Anthony D. Dutoi, Peter J. Love, and Martin Head-Gordon, Simulated quantum computation of molecular energies, *Science* **309**, 1704 (2005).
- [63] Trygve Helgaker, Sonia Coriani, Poul Jørgensen, Kasper Kristensen, Jeppe Olsen, and Kenneth Ruud, Recent advances in wave function-based methods of molecular-property calculations, *Chem. Rev.* **112**, 543 (2012).
- [64] Ryan Babbush, Dominic W. Berry, Ian D. Kivlichan, Annie Y. Wei, Peter J. Love, and Alán Aspuru-Guzik, Exponentially more precise quantum simulation of fermions in second quantization, *New J. Phys.* **18**, 033032 (2016).
- [65] Trygve Helgaker, Poul Jørgensen, and Jeppe Olsen, *Molecular Electronic-Structure Theory* (John Wiley and Sons, New York, 2013).
- [66] Michael A. Nielsen, The fermionic canonical commutation relations and the Jordan-Wigner transform, *School of Physical Sciences The University of Queensland* **59**, (2005).
- [67] Jarrod R. McClean *et al.*, OpenFermion: The electronic structure package for quantum computers, *Quantum Sci. Technol.* **5**, 034014 (2020).
- [68] Ville Bergholm *et al.*, PennyLane: Automatic differentiation of hybrid quantum-classical computations, [arXiv:1811.04968](https://arxiv.org/abs/1811.04968).
- [69] S. Debnath, N. M. Linke, C. Figgatt, K. A. Landsman, K. Wright, and C. Monroe, Demonstration of a small programmable quantum computer with atomic qubits, *Nature* **536**, 63 (2016).

- [70] Martin Larocca, Nathan Ju, Diego García-Martín, Patrick J. Coles, and Marco Cerezo, Theory of overparametrization in quantum neural networks, *Nat. Comput. Sci.* **3**, 542 (2023).
- [71] Jason D. Lee, Max Simchowitz, Michael I. Jordan, and Benjamin Recht, in *Conference on Learning Theory* (PMLR, New York, 2016), p. 1246.
- [72] Charles R. Harris *et al.*, Array programming with NumPy, *Nature* **585**, 357 (2020).
- [73] Norbert M. Linke, Dmitri Maslov, Martin Roetteler, Shantanu Debnath, Caroline Figgatt, Kevin A. Landsman, Kenneth Wright, and Christopher Monroe, Experimental comparison of two quantum computing architectures, *Proc. Natl. Acad. Sci. U.S.A.* **114**, 3305 (2017).
- [74] Sajjad Sanaei and Naser Mohammadzadeh, Qubit mapping of one-way quantum computation patterns onto 2D nearest-neighbor architectures, *Quantum Inf. Process.* **18**, 56 (2019).
- [75] F. Orts, E. Filatovas, G. Ortega, J. F. SanJuan-Estrada, and E. M. Garzón, Improving the number of T gates and their spread in integer multipliers on quantum computing, *Phys. Rev. A* **107**, 042621 (2023).
- [76] Stefan H. Sack, Raimel A. Medina, Alexios A. Michailidis, Richard Kueng, and Maksym Serbyn, Avoiding Barren Plateaus using Classical Shadows, *PRX Quantum* **3**, 020365 (2022).
- [77] Lucas Friedrich and Jonas Maziero, Avoiding barren plateaus with classical deep neural networks, *Phys. Rev. A* **106**, 042433 (2022).
- [78] Antonio A. Mele, Glen B. Mbeng, Giuseppe E. Santoro, Mario Collura, and Pietro Torta, Avoiding barren plateaus via transferability of smooth solutions in a Hamiltonian Variational Ansatz, *Phys. Rev. A* **106**, L060401 (2022).
- [79] Andrea Skolik, Jarrod R. McClean, Masoud Mohseni, Patrick van der Smagt, and Martin Leib, Layerwise learning for quantum neural networks, *Quantum Mach. Intell.* **3**, 1 (2021).
- [80] Henry Eyring, The activated complex in chemical reactions, *J. Chem. Phys.* **3**, 107 (1935).
- [81] Matthew P. A. Fisher, Peter B. Weichman, G. Grinstein, and Daniel S. Fisher, Boson localization and the superfluid-insulator transition, *Phys. Rev. B* **40**, 546 (1989).
- [82] Xin-Yu Huang, Lang Yu, Xu Lu, Yin Yang, De-Sheng Li, Chun-Wang Wu, Wei Wu, and Ping-Xing Chen, Qubitization of bosons, [arXiv:2105.12563](https://arxiv.org/abs/2105.12563).